

Article

A Novel Research on Behavior of Zinc Ferrite Nanoparticles in Different Concentration of Poly(vinyl pyrrolidone) (PVP)

Halimah Mohamed Kamari ^{1,*}, Mahmoud Goodarz Naseri ^{2,*} and Elias B. Saion ¹

¹ Department of Physics, Universiti Putra Malaysia, 43400 UPM Serdang, Selangor 43300, Malaysia; E-Mail: elias@science.upm.edu.my

² Department of Physics, Faculty of Science, Malayer University, Malayer 65719-95863, Iran

* Authors to whom correspondence should be addressed;

E-Mails: halimahmk@upm.edu.my (H.M.K.); mahmoud.naseri55@gmail.com (M.G.N.);

Tel.: +60-1-23906630 (H.M.K.); Fax: +60-3-89454454 (H.M.K.).

Received: 9 December 2013; in revised form: 28 February 2014 / Accepted: 4 March 2014 /

Published: 4 April 2014

Abstract: Zinc ferrite nanocrystals were prepared from an aqueous solution containing metal nitrates and various of concentrations of poly(vinyl pyrrolidone) (PVP), *i.e.*, 0, 15, 40, and 55 g/L, as a capping agent. To stabilize the particles, they were thermally treated at 873 K, as an optimum calcination temperature. The behaviors of the polymeric precursor were analyzed by use of simultaneous thermo-gravimetry (TG) and derivative thermo-gravimetry analyses (DTG). The presence of the crystalline phase in each sample was confirmed by X-ray diffraction (XRD) analysis. The average particle size and the morphology of the nanoparticles were determined by transmission electron microscopy (TEM), and these parameters were found to differ at various concentrations of PVP. Fourier transform infrared spectroscopy (FT-IR) confirmed the presence of metal oxide bands for all the PVP concentrations and confirmed the absence of organic bands for PVP concentrations less than 55 g/L. Measurements of the magnetization value of the zinc ferrite nanoparticles were obtained at room temperature by using a vibrating sample magnetometer (VSM), which showed that, in the absence of PVP, the sample exhibited a paramagnetic behavior while, in the presence of PVP, samples have a super-paramagnetic behavior.

Keywords: nanocrystals; magnetic properties; poly(vinyl pyrrolidone); thermal treatment

1. Introduction

The interest in research related to metal spinel ferrite nanoparticles, with the structure AB_2O_4 in which A and B pertain to tetrahedral and octahedral cation sites, respectively, and O indicates the oxygen anion site, has increased significantly in recent years. This is due to their potential applications in ferrofluids [1], magnetoptics [2], spintronics [3], biomedical applications [4,5], and anodes for batteries [6]. Various fabrication methods have been reported for preparing spinel ferrite nanocrystals for these purposes, e.g., sol-gel methods [7], the ball-milling technique [8], co-precipitation [9], the aerogel process [10], the hydrothermal method [11], the reverse micelles process [12], and the micro-emulsion method [13]. To overcome the drawbacks associated with the above-mentioned methods, organic and inorganic capping agents are used to stabilize the particles and prevent them from agglomerating. The properties of ferrite nanoparticles can be altered by controlling their size, which can provide an advantage in formulating new composite materials with optimized properties for various applications. Thus, to control the growth of the spinel ferrite nanoparticles, organic stabilizers (polymers), e.g., polyvinyl alcohol (PVA), polyethylene oxide (PEO), polymethacrylic acid (PMAA), and poly(vinyl pyrrolidone) (PVP), are added during the synthesis for capping the surface of the particles [14,15]. In our previous work [16], a thermal-treatment method was used to prepare zinc ferrite ($ZnFe_2O_4$) nanoparticles from an aqueous solution that contained metal nitrates, PVP, and deionized water. The preparation of the nanoparticles was followed by grinding and calcination at various temperatures from 723 to 873 K (see subsection 4.3 in [16]). In order to avoid the natural tendency to form aggregates, zinc ferrite nanoparticles were normally prepared or dispersed in PVP matrices. Currently, understanding the effect of capping nanoparticles is one of the most important topics in this area of research. Thus, in this work, the fundamental questions that we are attempting to address is how PVP caps zinc ferrite nanoparticles in aqueous solution containing metal nitrates and another, what amount is optimum (minimum) concentration of the PVP capping agent at which the nanoparticles are pure; also, this is the concentration at which the nanoparticles have the smallest particle size and a nearly uniform distribution of shapes.

2. Materials and Methods

2.1. Sample Preparation

Metal nitrate reagents, poly(vinyl pyrrolidone) (PVP), and deionized water were used as precursors. In addition, a capping agent (PVP) to control the agglomeration of the particles and a solvent (deionized water and metal nitrates) were used. Iron nitrate, $Fe(NO_3)_3 \cdot 9H_2O$, and zinc nitrate, $Zn(NO_3)_2 \cdot 6H_2O$, were purchased from Acros Organics with a purity exceeding 99%. PVP (MW = 29,000) was purchased from Sigma Aldrich and was used without further purification. In the next set of experiments, four separate aqueous solution of PVP were prepared by dissolving 0, 1.5, 4 and 5.5 g of polymer in 100 mL of deionized water at 363 K, before mixing 0.2 mmol iron nitrate and 0.1 mmol zinc nitrate (Fe:Zn = 2:1) into the polymer solution and constantly stirring for 2 h using a magnetic stirrer until a colorless, transparent solution was obtained. No precipitation of materials was observed before the heat treatment. The mixed solution was poured into a glass Petri dish and heated at 353 K in an oven for 24 h to evaporate the water. The dried, orange, solid zinc ferrite that remained

was crushed and ground in a mortar to form powder. The calcination of the powders was conducted at 873 K for 3 h for the decomposition of organic compounds and the crystallization of the nanocrystals.

2.2. Laboratory Determinations

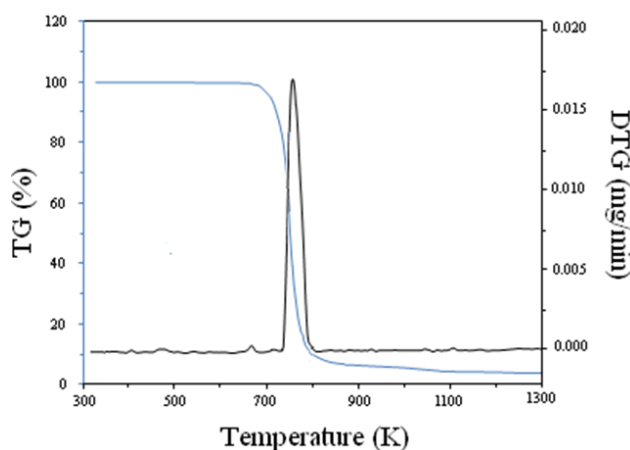
Thermal analyses (TG–DTG) including the thermogravimetry (TG) and derivative thermogravimetry (DTG) were carried out using a Perkin Elmer Thermal Analyzer model TGA7/DTA7 with the heating rate of 10° K/min under nitrogen atmosphere. The structure of the ZnFe₂O₄ nanoparticles was characterized by the XRD technique using a Shimadzu diffractometer meter model XRD 6000 employing Cu K_α (0.154 nm) radiation to generate diffraction patterns from powder crystalline samples at ambient temperature in a 2θ range of 10° to 70°. The microstructure and particle size of the nanocrystals were determined from Transmission Electron Microscopy (TEM) images that were obtained by using a JEOL 2010F, Ultrahigh Resolution (UHR), version electron microscope at an accelerating voltage of 200 kV. Fourier transform infrared spectroscopy (FT-IR) spectra were recorded using a PerkinElmer FT-IR model 1650 spectrometer (Labexchange, Swabian Burladingen, Germany). Before recording spectra, the samples were placed on a Universal ATR Sampling Accessory (diamond coated with CsI) and pressed, and then the spectra were recorded. Magnetization measurements were conducted using a vibrating sample magnetometer (VSM) (Lake Shore 4700, Lake Shore Cryotronics, Inc., Westerville, OH, USA) at room temperature with maximum magnetic field of 15 kOe.

3. Results and Discussion

3.1. Thermal Analyses of PVP

Figure 1 shows the simultaneous thermo-gravimetry (TG) and derivative thermo-gravimetry analyses (DTG) of PVP. It is evident that this polymer exhibited only one mass loss, which started at 678 K, and its maximum rate decomposition temperature was located at 778 K. This confirms that the majority of the mass loss occurs under 778 K and allows for the optimization of the heat treatment program. It is worth noting that several authors reported the thermal degradation of PVP exhibiting only one mass loss [17–19].

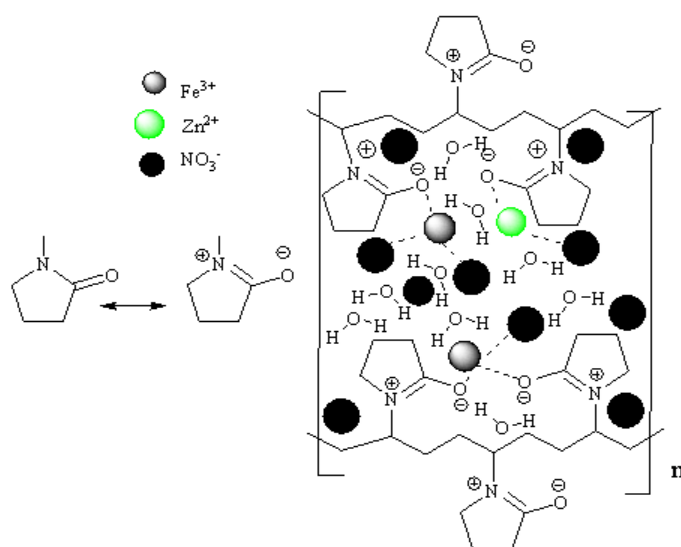
Figure 1. Thermal analyses of the polymeric precursor obtained by TG-DTG technique.



3.2. Mechanism of Formation

Interactions between the PVP capping agent [20] and metal ions are shown schematically in Figure 2, which shows that the zinc (II) and iron (III) ions are bound by the strong ionic bonds between the metallic ions and the amide group in a polymeric chain. PVP acts as a stabilizer for dissolved metallic salts through steric and electrostatic stabilization of the amide groups of the pyrrolidine rings and the methylene groups. Initially, the PVP stabilizer may decompose to a limited extent, thereby producing shorter polymer chains that are capped when they are adsorbed onto the surfaces of metallic ions [21]. The metallic ions, which are well dispersed in the cavities and networks, are created as a result of the shorter polymer chains. These mechanisms continue until they are terminated by the drying step. The influence of PVP is not restricted only to the solution and the drying step; PVP also affects the formation of the nuclei (*i.e.*, nucleation) of the zinc ferrite nanoparticles in the calcination step. In this step, the small nanoparticles with high surface energy levels would become larger via the Ostwald ripening process [22] without the presence of PVP, disrupt steric hindrance, thereby preventing their aggregation. Steric hindrance is a phenomenon that is attributed to large molecular weight (>10,000) and the repulsive forces acting among the polyvinyl groups [23,24]. These interactions are similar to the stabilization of metallic nanoparticles, *i.e.*, silver and gold [25,26].

Figure 2. The proposed mechanism of interaction between PVP and metal ions in the formation of the zinc ferrites nanoparticles.



3.3. Effect of Calcination Temperature on Phase Composition, Morphology and Magnetic Properties

In this subsection, we briefly report the results of our previous work [16] where the authors investigated on effect of calcinations temperature on phase composition, morphology and magnetic properties of zinc ferrite nanoparticles. In previous work [16], when precursors of zinc ferrite nanoparticles were calcined at 723, 773, 823, and 873 K, the particle sizes of zinc ferrite nanoparticles increased to 17, 22, 27, and 31 nm, respectively, as confirmed by TEM and XRD analyses. A completed crystallization occurred at 873 K, as were deduced by the absence of organic absorption bands in the FT-IR spectrum. Magnetic results were obtained by vibrating sample magnetometer

(VSM), and they showed that saturation magnetization decreased when the particle sizes increased, whereas the coercivity field was negligible, and all the samples displayed superparamagnetic behaviour. Optimum calcination temperature of zinc ferrite nanoparticles, occurred at 873 K, because this temperature was the minimum temperature at which the nanoparticles were pure; also, this was the temperature at which the nanoparticles had the smallest particle size and a nearly uniform distribution of shapes.

3.4. Effect of Concentration of PVP on Phase Composition, Morphology and Magnetic Properties

Figure 3 shows the XRD peaks of zinc ferrite nanoparticles that were prepared with concentrations of PVP, ranging from 0 to 55 g/L, and calcined at 873 K. It is important to note that, in thermal treatment method, the optimum temperature for the calcination of zinc ferrite nanoparticles was 873 K, because this temperature was the minimum temperature at which the nanoparticles were pure; also, this is the temperature at which the nanoparticles have the smallest particle size and a nearly uniform distribution of shapes [16]. It is evident from Figure 3 that the patterns show the reflection planes (111), (220), (311), (222), (400), (331), (422), (511), and (440), which confirm the presence of single-phase ZnFe_2O_4 with a face-centered cubic structure [27]. Except for the impure phases of $\alpha\text{-Fe}_2\text{O}_3$ and ZnO , which are found in all calcined samples and occur naturally as hematite and zincite, respectively [28], the remaining peaks correspond to the standard pattern of ZnFe_2O_4 (cubic, $a = 0.8441$ nm, space group: $\text{Fd}3\text{m}$, $Z = 8$; ICDD PDF: 22-1012).

Figure 3. XRD patterns of zinc ferrite nanoparticles with concentration of (a) 0, (b) 15, (c) 40, and (d) 55 g/L which calcined at 873 K.

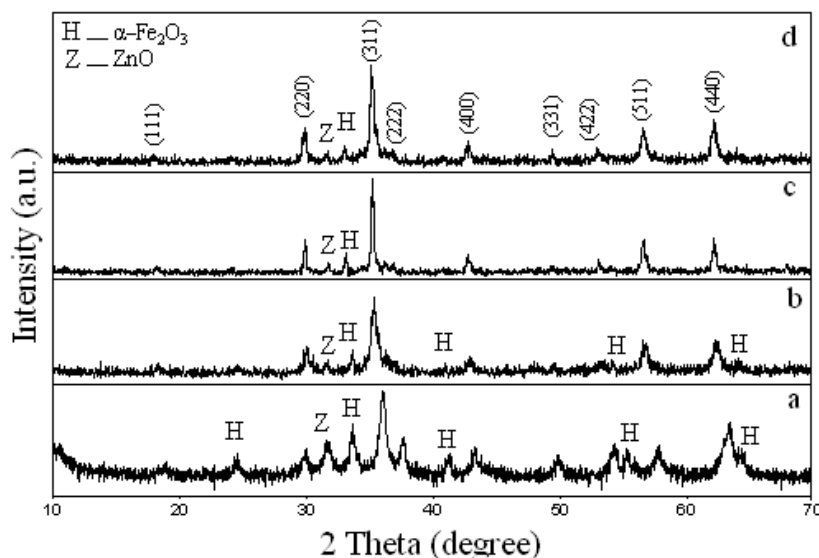


Table 1 shows percentages of hematite ($\alpha\text{-Fe}_2\text{O}_3$), zincite (ZnO) phases and spinel phase (ZnFe_2O_4) of samples with various concentration from 0 to 55 g/L which were estimated by X' Pert HighScore software (Philips, Almelo, The Netherlands). The highest percentages of hematite (27.3 vol%) and zincite (5.4 vol%) phases occurred in the absence of PVP while the lowest percentage of spinel phase (67.3 vol%) was obtained. When concentration of PVP increased from 15 to 55 g/L, the percentages of hematite and zincite phases decreased from 4.8 and 0.8 vol% to 1.6 and 0.5 vol% while spinel phase

increased from 94.4 to 97.9 vol%. This confirmed that the presence of PVP significantly improved the percentage of spinel phase or the degree of crystallinity of these products.

Table 1. Phase composition and average particle size (nm) of ZnFe₂O₄ nanoparticles with various concentrations of poly(vinyl pyrrolidone) (PVP) determined by X-ray diffraction (XRD) and transmission electron microscopy (TEM) techniques calcined at 873 K.

ZnFe ₂ O ₄ nanoparticles	Concentrations of PVP (g/L)	Percentage of hematite phase, vol.%	Percentage of zincite phase, vol.%	Percentage of spinel phase, vol.%	Particle size XRD (nm)	Particle size TEM (nm)
ZnFerrite 1	0	27.3	5.4	67.3	-	-
ZnFerrite 2	15	4.8	0.8	94.4	29	28 ± 2
ZnFerrite 3	40	1.7	0.5	97.8	33	31 ± 11
ZnFerrite 4	55	1.6	0.5	97.9	35	34 ± 9

The average particle size was determined from the full width at the half maximum (FWHM) of the XRD patterns, using the well-known Scherer formula:

$$D = 0.9\lambda/\beta\cos\theta \quad (1)$$

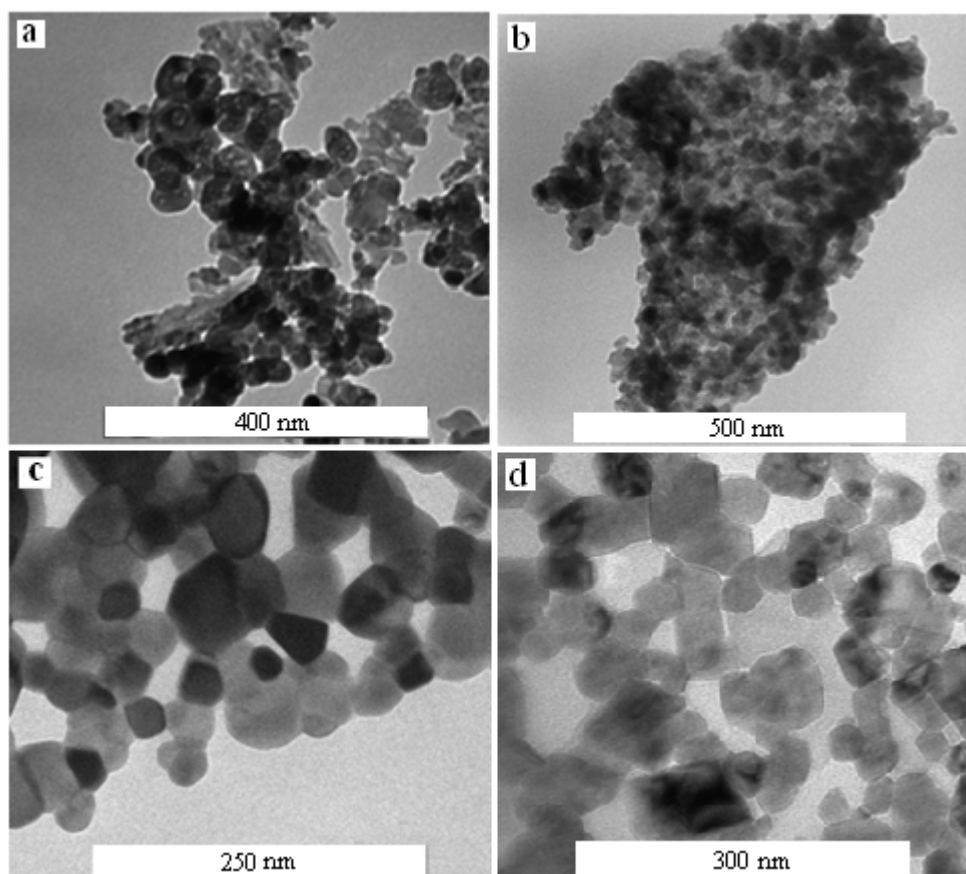
where D is the crystallite size (nm), β is the full width of the diffraction line at half of the maximum intensity measured in radians, λ is the X-ray wavelength of Cu K α = 0.154 nm, and θ is the Bragg angle [29]. The particle sizes estimated using the Scherer formula were found to increase with the concentration of PVP, from 15 to 55 g/L as shown in Table 1.

A comparison of XRD peaks shows that either the numbers or the intensities of the unwanted peaks of α -Fe₂O₃ and ZnO increase in the absence of PVP, but when PVP is present at concentrations of 15, 40 and 55 g/L, either remove some of the unwanted peaks (α -Fe₂O₃ and ZnO) or decrease the intensities of the some of them. This could be due to the fact that decreasing the concentration of PVP results in increases in the concentrations of zinc and iron ions [30]. In fact, due to the absence of PVP, there is no interaction between ferrite and PVP chains, which resulted in increasing either the numbers or the intensities of the unwanted peaks of α -Fe₂O₃ and ZnO [31]. Therefore, one of the important roles of PVP in synthesis of zinc ferrite nanoparticles by the thermal treatment method is the enhancement of the degree of the crystallinity by decreasing or removing α -Fe₂O₃ and ZnO.

To further investigate the role of PVP in the synthesis of zinc ferrite nanoparticles, we have shown, the TEM images and the FT-IR spectra of zinc ferrite nanoparticles with various concentrations of 0, 15, 40 and 55 g/L (Figures 4 and 5). Figure 4a shows that zinc ferrite nanoparticles were formed even in the absence of PVP. However, in this case, it was observed that the nanoparticles did not have a uniform distribution of shapes, and they were aggregated extensively and, in some areas, completely disproportionately distributed. Thus, without the use of PVP in the synthesis of nanoparticles, the small nanoparticles aggregate and produce larger nanoparticles [24] due to high surface energy (as shown earlier in Figure 2). When the concentration of PVP was increased to 15 g/L, the zinc ferrite nanoparticles that were formed with average size of 28 nm became more regular in shape than in the case without PVP (Figure 4b). However, due to the low concentration of PVP, these nanoparticles also aggregated because there was insufficient PVP to cap them well and prevent their agglomeration.

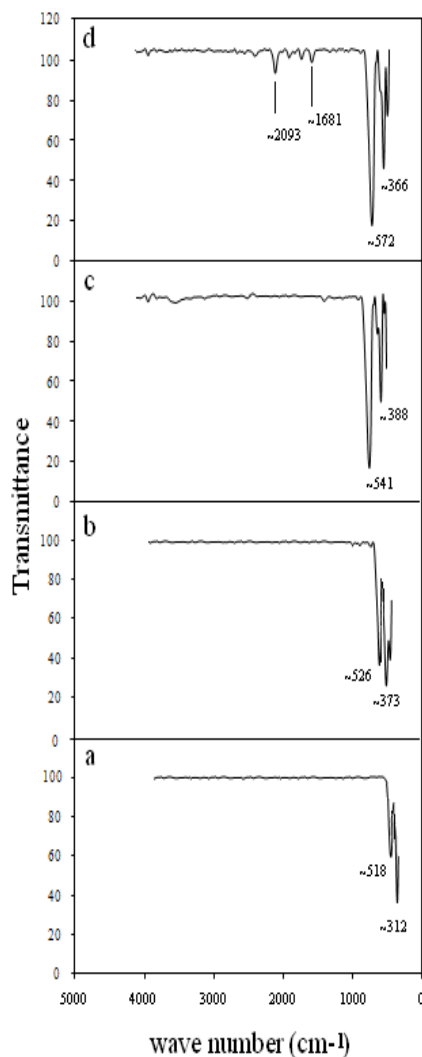
By increasing the PVP concentration to 55 g/L, the zinc ferrite nanoparticles did not agglomerate, and they were nearly uniform in shape, as shown in Figure 4d. However, in this case, the zinc ferrite nanoparticles ranged in size from $(34 - 9)$ to $(34 + 9)$ nm. These results were similar to the results achieved when a PVP concentration of 40 g/L was used (shown in Figure 4c).

Figure 4. TEM images of zinc ferrite nanoparticles with concentration of (a) 0, (b) 15, (c) 40, and (d) 55 g/L, which calcined at 873 K.



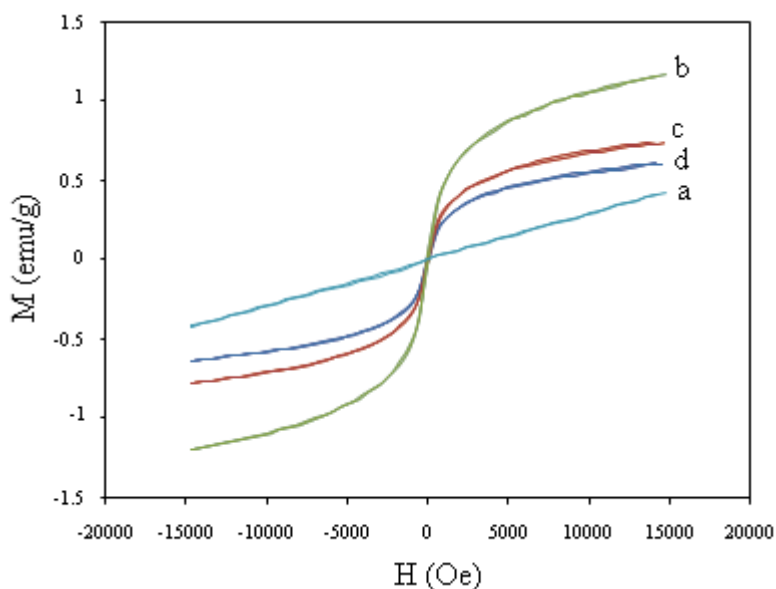
Two main broad metal–oxygen bands are seen in Figure 5 in the IR spectra of all spinel ferrite nanoparticles, which correspond to intrinsic stretching vibrations of the metal at the tetrahedral site, $M_{\text{tetra}} \leftrightarrow O$ (observed from 518 to 572 cm^{-1}) and octahedral-metal stretching, $M_{\text{octa}} \leftrightarrow O$ (observed from 312 to 388 cm^{-1}) [32]. However, due to the high concentration of PVP, traces of organic materials were observed at 1681 and 2093 cm^{-1} , which were associated with C=O and CO₂ stretching vibration respectively [33] as shown in Figure 5d. Thus, in fact, it is apparent that the zinc ferrite nanoparticles were contaminated with organic compounds in this case. However, in the absence of PVP and with concentrations of less than 55 g/L, the fabricated zinc ferrite nanoparticles were pure as shown in Figure 5a–c. Therefore, in the thermal treatment method, the optimum concentration of PVP for the synthesis of zinc ferrite nanoparticles is 40 g/L. That concentration, in combination with the optimum temperature (873 K) provided the conditions required to fabricate pure zinc ferrite nanoparticles that have the smallest particle size.

Figure 5. FT-IR spectra of zinc ferrite nanoparticles with concentrations of (a) 0, (b) 15, (c) 40, and (d) 55 g/L, which calcined at 873 K.



Eventually, the magnetization curves of zinc ferrite nanoparticles with various concentrations of PVP from 0, 15, 40, and 55 g/L, were represented at room temperature in the range of approximately -15 to $+15$ kOe (Figure 6). These curves exhibited different magnetic behaviors so that, in absence of PVP zinc ferrite displayed paramagnetic behavior while in presence of PVP, with concentration of 15, 40 and 55 g/L; they behaved such as a super paramagnet at room temperature. As was discussed in Figure 4a, in absence of PVP, zinc ferrite did not have a uniform distribution of shapes, and they were aggregated such as a bulk. In bulk form, zinc ferrite has a normal spinel structure in which all Zn^{2+} ions are in A sites and Fe^{3+} ions are distributed in B sites and it is antiferromagnetic below 10 K and paramagnetic above this temperature [34]. However, in bulk, zinc ferrite only occurs in intra-sub-lattice (B–B) exchange interactions, and it does not have intra-sub-lattice (A–A) exchange interactions or inter-sub-lattice (A–B) super-exchange interactions [35]. Inter-sub-lattice (A–B) super-exchange interactions of the cations are much stronger than the (A–A) and (B–B) interactions [7].

Figure 6. Magnetization curve at room temperature for zinc ferrite nanoparticles with concentration of (a) 0, (b) 15, (c) 40, and (d) 55 g/L, which calcined at 873 K.



By increasing the amount of PVP, from 15 to 55 g/L the saturation magnetization decreased from 1.1 to 0.65 emu/g (as listed in Table 2) whereas the coercivity field was negligible, and all of the samples displayed super-paramagnetic behaviors.

Table 2. Magnetic properties of ZnFe_2O_4 nanoparticles with various concentrations of PVP, determined by vibrating sample magnetometer (VSM) technique at room temperature, calcined at 873 K.

ZnFe_2O_4 nanoparticles	Concentrations of PVP (g/L)	Saturation magnetization M_s (emu/g)
ZnFerrite 1	0	0.43
ZnFerrite 2	15	1.1
ZnFerrite 3	40	0.74
ZnFerrite 4	55	0.60

Due to the degree of inversion, which is large for smaller size particles (lower concentration of PVP), inter-sublattice (A–B) super-exchange interactions in smaller size particles occur to a greater extent than in larger size particles (higher concentration of PVP) [16].

4. Conclusions

This work investigated a comprehensive research on the amazing effects and role of PVP in the synthesis of zinc ferrite nanoparticles by the thermal treatment method. Briefly, as was discussed when we considered our XRD results, TEM images, FT-IR spectra, and VSM results, PVP plays five crucial roles in synthesizing zinc ferrite nanoparticles, *i.e.*, (1) the control of the growth of the nanoparticles; (2) the prevention of agglomeration of the nanoparticles; (3) the enhancement of the degree of the crystallinity of the nanoparticles; (4) the production of nanoparticles that have a uniform distribution of shapes; and (5) the transition of samples from the paramagnetic phase to the super paramagnetic phase

at room temperature. Optimum concentration of PVP (40 g/L) was obtained because of the fact that, this concentration was the minimum concentration at which the nanoparticles were pure; also, this was the concentration at which the nanoparticles had the smallest particle size and a nearly uniform distribution of shapes.

Conflicts of Interest

The authors declare no conflict of interest.

References

1. Rosensweig, R.E. *Ferrohydrodynamics*; Dover: New York, NY, USA, 1985.
2. Tirosch, E.; Shemer, G.; Markovich, G. Optimizing cobalt ferrite nanocrystal synthesis using a magneto-optical probe. *Chem. Mater.* **2006**, *18*, 465–470.
3. Luders, U.; Barthelemy, A.; Bibes, M. NiFe₂O₄: A versatile spinel magterial brings new opportunities for Spintronics. *Adv. Mater.* **2006**, *18*, 1733–1736.
4. Pankhurst, Q.A.; Connolly, J.; Jones, S.K. Applications of magnetic nanoparticles in biomedicine. *J. Phys. D* **2003**, *36*, R167–R181.
5. Berry, C.C. Possible exploitation of magnetic nanoparticles-cell interaction for biomedical applications. *J. Mater. Chem.* **2005**, *15*, 543–547.
6. Selvan, R.K.; Kalaiselvi, N.; Augustin, C.O. SnO₂ pinning: An approach to enhance the electrochemical properties of anodes for batteries. *Electrochem. Solid State Lett.* **2006**, *9*, A390–A394.
7. Atif, M.; Hasanian, S.K.; Nadeem, M. Magnetization of sol-gel prepared zinc ferrite nanoparticles: Effects of inversion and particle size. *J. Sci. Commun.* **2006**, *138*, 416–421.
8. Jiang, J.Z.; Wynn, P.; Morup, S. Magnetic structure evolution in mechanically milled nanostructured ZnFeO₂ particles. *Nanostruct. Mater.* **1999**, *12*, 737–740.
9. Shenoy, S.D.; Joy, P.A.; Anantharaman, M.R. Effect of mechanical milling on the structural, magnetic and dielectric properties of coprecipitated ultrafine zinc ferrite. *J. Magn. Magn. Mater.* **2004**, *269*, 217–226.
10. Hamdeh, H.H.; Ho, J.C.; Oliver, S.A.; Willey, R.J.; Oliveri, G.; Busca, G. Magnetic properties of partially-inverted zinc ferrite aerogel powders. *J. Appl. Phys.* **1997**, *81*, 1851–1858.
11. Yu, S.H.; Fujino, T.; Yoshimura, M. Hydrothermal synthesis of ZnFe₂O₄ ultrafine particles with high magnetization. *J. Magn. Magn. Mater.* **2003**, *256*, 420–427.
12. Morrison, S.A.; Cahill, C.L.; Carpenter, E.E. Magnetic and structural properties of nickel zinc ferrite nanoparticles synthesized at room temperature. *J. Appl. Phys.* **2004**, *95*, 6392–6395.
13. Hochepped, J.P.; Bonville, J.F.; Pileni, M.P. Non stoichiometric zinc ferrite nancrystals: Syntheses and magnetic properties. *J. Phys. Chem.* **2000**, *104*, 905–912.
14. Rana, S.; Gallo, A.; Srivastava, R.S. On the suitability of nanocrystalline ferrites as a magnetic carrier for drug delivery: Functionalization, conjugation, and drug release behavior. *Acta Biomater.* **2007**, *3*, 233–242.

15. Naseri, M.G.; Saion, E.B.; Abbastabar, A.H.; Hashim, M.; Shaari, A.H. Simple preparation and characterization of nickel ferrite nanocrystals by a thermal treatment method. *Powder Technol.* **2011**, *212*, 80–88.
16. Naseri, M.G.; Saion, E.B.; Hashim, M.; Shaari, A.H.; Ahangar, H.A. Synthesis and characterization of zinc ferrite nanoparticles by a thermal treatment method. *Solid State Commun.* **2011**, *151*, 1031–1035.
17. Kumar, S.V.; Musturappa, T.E.; Prasannakumar, S.; Mahadevan, K.M.; Sherigara, B.S. *N*-Vinylpyrrolidone and ethoxyethyl methacrylate copolymer: Synthesis, characterization and reactivity ratios. *J. Macromol. Sci. Part A* **2007**, *44*, 1161–1169.
18. Silva, M.F.; Silva, C.A.; Fogo, F.C.; Pineda, E.A.G.; Hechenleitner, A.A.W. Thermal and FTIR study of polyvinylpyrrolidone/lignin blends. *J. Ther. Anal. Calorim.* **2005**, *79*, 367–370.
19. Lau, C.; Mi, Y. A study of blending and complexation of poly(acrylic acid)/poly(vinyl pyrrolidone). *Polymer* **2002**, *43*, 823–829.
20. Sivakumar, P.; Ramesh, R.; Ramanand, A. Synthesis and characterization of NiFe₂O₄ nanosheet via polymer assisted co-precipitation method. *Mater. Lett.* **2011**, *65*, 483–485.
21. Koebel, M.M.; Jones, L.C.; Somorjai, G.A. Preparation of size-tunable, highly monodisperse PVP-protected Pt-nanoparticles by seed-mediated growth. *J. Nanopart. Res.* **2008**, *10*, 1063–1069.
22. Roosen, A.R.; Carter, W.C. Simulations of microstructural evolution: Anisotropic growth and coarsening. *Phys. A* **1998**, *261*, 232–247.
23. Ghosh, G.; Naskar, M.K.; Patra, A. Synthesis and characterization of PVP-encapsulated ZnS nanoparticles. *Opt. Mater.* **2006**, *28*, 1047–1053.
24. Shao, H.; Hi, Y.; Lee, H. Effect of PVP on the morphology of cobalt nanoparticles prepared by thermal decomposition of cobalt acetate. *Curr. Appl. Phys.* **2006**, *6*, e195–e197.
25. Huang, W.; Xu, G. Characterization of nano-Ag/PVP composites synthesized via ultra-violet irradiation. *J. Coal Sci. Eng.* **2010**, *16*, 188–192.
26. Tsuji, M.; Hashimoto, M.; Nishizawa, Y.; Tsuji, T. Synthesis of gold nanorods and nanowires by microwave-polyol method. *Mater. Lett.* **2004**, *58*, 2326–2330.
27. Chinnasamy, C.N.; Ponpandian, A.N.; Chattopadhyay, K.; Guerault, H.; Greneche, J.M. Magnetic properties of nanostructured ferrimagnetic zinc ferrite. *J. Phys.* **2000**, *12*, 7795–7805.
28. Laokul, P.; Amornkitbamrung, V.; Seraphin, S. Characterization and magnetic properties of nanocrystalline CuFe₂O₄, NiFe₂O₄, ZnFe₂O₄ powders prepared by the Aloe vera extract solution. *Curr. Appl. Phys.* **2011**, *11*, 101–108.
29. Cullity, B.D. *Elements of X-ray Diffraction*; Addison-Wesley: London, UK, 1987.
30. Sharma, D.R.; Mathur, R.; Vadera, S.R. Synthesis of nanocomposites of Ni–Zn ferrite in aniline formaldehyde copolymer and studies on their pyrolysis products. *J. Alloys Compd.* **2003**, *358*, 193–204.
31. Elsayed, A.H.; Mohy Eldin, M.S.; Elsyed, A.M. Synthesis and properties of polyaniline/ferrites nanocomposites. *Int. J. Electrochem. Sci.* **2011**, *6*, 206–221.
32. Niasari, M.S.; Davar, F.; Mahmoudi, T. A simple route to synthesize nanocrystalline nickel ferrite (NiFe₂O₄) in the presence of octanoic acid as a surfactant. *Polyhedron* **2009**, *28*, 1455–1458.

33. Nyutu, E.K.; Canner, W.C.; Auerbach, S.M.; Chen, C.H.; Suib, S.L. Ultrasonic nozzle spray *in situ* mixing and microwave-assisted preparation of nanocrystalline spinel metal oxides: Nickel ferrite and zinc aluminate. *J. Phys. Chem. C* **2008**, *112*, 1407–1414.
34. Mathew, D.S.; Juang, R.S. An overview of the structure and magnetism of spinel ferrite nanoparticles and their synthesis in microemulsions. *Chem. Eng. J.* **2007**, *129*, 51–65.
35. Li, F.S.; Wang, L.; Wang, J.B.; Zhou, Q.G.; Zhou, X.Z.; Kunkel, H.P.; Williams, G. Site preference of Fe in nanoparticles of $ZnFe_2O_4$. *J. Magn. Magn. Mater.* **2004**, *268*, 332–339.

© 2014 by the authors; licensee MDPI, Basel, Switzerland. This article is an open access article distributed under the terms and conditions of the Creative Commons Attribution license (<http://creativecommons.org/licenses/by/3.0/>).